Elliptic flow parameter and its fluctuation in ^{197}Au + ^{197}Au collisions at the STAR-BES energies in a multiphase transport model

Joydeep Thakur, Provash Mali, and Amitabha Mukhopadhyay*
Department of Physics, University of North Bengal, Siliguri, West Bengal 734013, India

(Received 6 November 2023; revised 24 May 2024; accepted 27 June 2024; published 22 July 2024)

We study the elliptic flow parameter and its event-by-event fluctuation in ^{197}Au + ^{197}Au collisions at energies used in the STAR Beam Energy Scan (phase I) program, while using the string melting version of a multiphase transport (AMPT) model as a baseline prediction. We employ different methods to determine the elliptic flow parameter, compare their values with each other, and study their dependencies on the collision centrality, transverse momentum, pseudorapidity, and nucleon-nucleon center of mass energy. Within the framework of the AMPT model, we examine how the nonflow effects arising out of interparticle correlations influence the values of the elliptic flow parameter. We also study the centrality and energy dependencies of the event-by-event fluctuation of elliptic flow, and compare our simulation results with the STAR experimental data wherever they are available. We observe that the simulation can reasonably well reproduce the shape of the centrality dependence of the elliptic flow and its fluctuation as seen in the experiment. However, the simulation slightly underestimates the integrated values of the elliptic flow parameter, and it does not quite match with the transverse momentum and pseudorapidity dependencies observed in the experiment. We also observe that the contribution of nonflow effects to the centrality dependence of elliptic flow and its fluctuation is marginal. Fluctuations in the elliptic flow depend nonmonotonically on the collision energy involved, in the experiment as well as in the simulation.

DOI: 10.1103/PhysRevC.110.014909

I. INTRODUCTION

One of the main objectives of studying nuclear matter under extreme thermodynamic conditions is to explore various properties of the strongly interacting fireball medium produced in high-energy nucleus-nucleus collisions. It is believed that the azimuthal anisotropy of the final state particle distributions, if any, can be used to characterize several aspects of the nucleus-nucleus collision dynamics and to explore a collective fluidlike property of the fireball [1–4]. The periodic nature of the azimuthal distribution of charged hadrons can be decomposed into a Fourier series [5]. The Fourier coefficient denoted by v_n is called the nth order flow harmonic. The second harmonic coefficient, known as the elliptic flow parameter (v_2), is of particular interest, because it allows us to critically examine the evolution of the early stages of a nucleus-nucleus collision process [6]. The initial spatial anisotropy of the coordinate distribution of the nucleons present within the overlapping part of the colliding nuclei, nearly ellipsoid in shape, and the pressure gradient developed thereof, are predominantly responsible for the development of elliptic flow in the final state. The initial anisotropy is transferred to the final state particles via strongly interacting constituents of the fireball.

Estimation of v_2 from the distribution of azimuthal angles (ϕ) of charged hadrons is either influenced by the event-by-event (e-by-e) fluctuation of v_2 or is biased by the nonflow effects that are not related to the participant plane geometry [7], like resonance decay, jet fragmentation, and Hanbury Brown and Twiss correlation. The PHOBOS collaboration has reported that the relative fluctuation of v_2 measures approximately 40–50% of the v_2 value itself [8]. Due to the fluctuations in the number and position coordinates of the participating nucleons, the eccentricity (ε_2) of the overlapping region of the impinging nuclei, even within the same centrality class, may also fluctuate on an e-by-e basis. Fluctuations in the initial geometry seem to drive the hydrodynamic evolution of the nucleus-nucleus collision system on an average as well as on an e-by-e basis. However, it has been suggested that v_2 fluctuations can be used to probe the early stage dynamics of nucleus-nucleus collision, even without considering any fluctuation of the initial state [9].

In this paper we study the v_2 parameter as a function of collision centrality, transverse momentum (p_T), pseudorapidity (η) and center of mass energy ($\sqrt{s_{\rm NN}}$), and the e-by-e fluctuation of v_2 as a function of collision centrality and $\sqrt{s_{\rm NN}}$ for the charged hadrons produced in ^{197}Au + ^{197}Au collisions. Our analysis pertains to $\sqrt{s_{\rm NN}} = 7.7$, 11.5, 19.6, 27.0, and 39.0 GeV, energies that are used in phase I of the STAR BES program at the RHIC of Brookhaven National Laboratory [10]. We also extrapolate our simulation study on ^{197}Au + ^{197}Au collision to $\sqrt{s_{\rm NN}} = 62.4$ GeV, another energy value previously used by the STAR collaboration. We employ the AMPT model in its string melting (AMPT-SM) configuration [11], apply the same kinematic cuts to the simulated data as

*Contact author: amphys@nbu.ac.in

 ©2024 American Physical Society

they are in the experiments, and compare each experiment with the respective simulation wherever the results are available. We adopt various methods to calculate the v_2 values. In the framework of the AMPT-SM model we study the nonflow effects and take care of the self-correlation while examining the centrality dependence of v_2. The objective of this analysis is to compare the v_2 results obtained from different methods with each other and examine to what extent the same can be reproduced by the AMPT simulation. In Sec. II we explain different methods adopted in this analysis to determine v_2. In Sec. III the AMPT model has been briefly outlined. In Sec. IV we present and discuss the results of the STAR experiment on elliptic flow and its e-by-e fluctuation, while using the predictions of AMPT-SM as a reference baseline. In Sec. V we conclude with a summary of our major observations.

II. METHODOLOGY

Several methods to determine v_2 have been proposed [12–16]. They are sensitive in varying degrees to the flow fluctuations and nonflow contributions that are responsible for additional correlations not related to the participant or reaction plane. Here we have adopted four different methods to calculate v_2. Without claiming any originality in this regard, a brief description of these methods is outlined in this section.

A. The participant plane method

The ϕ distribution of charged hadrons in the final state is anisotropic and periodic in nature. As mentioned earlier, it can be decomposed into a Fourier series [12] like

$$\frac{dN_{ch}}{d\phi} \propto \left[1 + 2\sum_{n=1}^{\infty} v_n \cos\{n(\phi - \Psi_{\rm RP})\}\right]. \tag{1}$$

For an event, the nth order flow coefficient v_n is given by

$$v_n = \langle \cos[n(\phi - \Psi_{\rm RP})]\rangle. \tag{2}$$

Here $\Psi_{\rm RP}$ denotes the azimuthal angle of the reaction plane, a plane subtended by the impact parameter of the collision and the incident beam direction. $\langle\ \rangle$ denotes an averaging over all particles involved, charged hadrons in the present case. In commonly used transport models like the AMPT [11], the impact parameter and the beam direction are taken, respectively, along the x and z axis. In the AMPT framework the reaction plane angle is thus predefined to be zero. In real experiments, however, the direction of the impact parameter cannot be determined. Measuring $\Psi_{\rm RP}$ is therefore not possible. An alternative way to determine the flow parameters is to use the nth order participant plane angle ψ_n given by

$$\psi_n = \frac{1}{n}\left[\arctan\frac{\langle r^2\ \sin(n\varphi)\rangle}{\langle r^2\ \cos(n\varphi)\rangle} + \pi\right] \tag{3}$$

where $(r,\ \varphi)$ are the coordinates of the participating nucleons. In simulation studies like ours, they are obtained by using the Monte Carlo Glauber (MCG) model [17]. It has been suggested that Eq. (1) can still be used. However, ψ_n should be calculated in the center of mass system of the participating nucleons. Now $\langle\ \rangle$ denotes a density weighted average over the initial states [18,19]. Flow parameters measured with respect to the participant plane are therefore given by

$$v_n\{PP\} = \langle \cos[n\{\phi - \psi_n\}]\rangle \tag{4}$$

where the e-by-e fluctuation of the nucleons directly participating in a collision is also taken into account. Corresponding geometrical anisotropy of the initial state, i.e., the overlapping part of the colliding nuclei, is measured by an eccentricity parameter like

$$\varepsilon_n\{PP\} = \frac{\sqrt{\langle r^n \cos n\varphi\rangle^2 + \langle r^n \sin n\varphi\rangle^2}}{\langle r^n\rangle}. \tag{5}$$

However, in real experiments r has to be replaced by p_T and the coordinate space φ by the corresponding momentum space angle, replacements that do not significantly change the flow parameter values [19].

B. The event plane method

In experiments neither $\Psi_{\rm RP}$ nor ψ_n can be directly measured. One can bypass the problem by using an event flow vector Q_n, defined in terms of an event plane angle Ψ_n for the nth flow harmonic as [12]

$$\begin{aligned} Q_n\ \cos(n\Psi_n) &= Q_{n_x} = \sum_i w_i\ \cos n\phi_i, \\ Q_n\ \sin(n\Psi_n) &= Q_{n_y} = \sum_i w_i\ \sin n\phi_i, \\ \Psi_n &= \tan^{-1}\left(\frac{Q_{n_y}}{Q_{n_x}}\right)/n. \end{aligned} \tag{6}$$

Here w_i and ϕ_i, respectively, denote a weight factor and the azimuthal angle associated with the ith particle, and the sum over i runs for all particles of an event except those used to determine v_2. For example, in our simulation based analysis π^0 mesons are used to determine Q_n and Ψ_n, whereas v_2 is obtained only for the charged hadrons. Each sine and cosine term present in the summations of Eq. (6) is weighted by the p_T value of the respective π^0 meson. The observed v_2 is calculated as

$$v_2^{\rm obs} = \langle \cos[2(\phi - \Psi_2)]\rangle \tag{7}$$

where the sum is taken over all particles and all events concerned. The most dominant nonflow effect arises from two-particle correlation, which scales with the inverse of the multiplicity of particles that are used to determine the event plane [12]. The second harmonic of Eq. (1) is then obtained after dividing $v_2^{\rm obs}$ by the event plane resolution [5,20] as

$$v_2\{EP\} = \frac{v_2^{\rm obs}}{\langle \cos\{2(\Psi_2 - \Psi_{\rm RP})\}\rangle}. \tag{8}$$

The event plane resolution can be determined by dividing an event into two subevents, say A and B that in our case are separated by an η gap, $\Delta\eta = 0.15$. Following [12] we then have

$$v_2\{EP\} = \frac{v_2^{\rm obs}}{\sqrt{2\left\langle \cos\left\{2\left(\Psi_2^A - \Psi_2^B\right)\right\}\right\rangle}} \tag{9}$$

where Ψ_2^A and Ψ_2^B are the event plane angles of the respective subevents.

C. The cumulant methods

The difficulty associated with the experimental measurement of $\Psi_{\rm RP}$ or ψ_n can also be resolved by using the n-particle correlation, an aspect that is widely studied in the particle emission process in high-energy collisions. Recently, the Q-cumulant method has been introduced for flow analysis, which is used to determine the flow parameters from higher order particle correlations [15,21]. The nth order azimuthal correlation is expressed in terms of the Q vector as

$$Q_n = \sum_{j=1}^{M} e^{in\phi_j} \tag{10}$$

where M denotes the multiplicity of the selected set of particles in an event, and ϕ_j denotes their azimuthal angles. The average two-particle azimuthal correlation $\langle 2\rangle$ for all particles in an event is then calculated as

$$\langle 2\rangle = \frac{|Q_n|^2 - M}{M(M-1)}. \tag{11}$$

The two-particle cumulant $c_n\{2\}$ and the anisotropic flow parameter $v_n\{2\}$ are obtained after averaging over all events as

$$c_n\{2\} = \langle\langle 2\rangle\rangle \quad \text{and } v_n\{2\} = \sqrt{c_n\{2\}}. \tag{12}$$

Unfortunately, $v_n\{2\}$ obtained in this way contains contributions from different nonflow effects described earlier. These nonflow effects, generally short ranged in nature, can be suppressed by introducing a gap on the pseudorapidity axis among the particles used in the two-particle Q-cumulant method [22]. For this purpose once again we divide an event into two subevents L and R within the η ranges $-1.0 > \eta > -0.5$ and $0.5 > \eta > 1.0$, respectively, so that an η gap of at least $|\Delta\eta| = 1.0$ is inserted between any two particles each taken from each subevent. In nucleus-nucleus collisions the short-ranged correlation (SRC) usually extends over a small rapidity gap ($\Delta y < 1.0$) [23]. Equation (11) is then modified as

$$\langle 2\rangle_{\Delta\eta} = \frac{Q_n^L Q_n^{R*}}{M_L M_R} \tag{13}$$

where Q_n^L and Q_n^R are, respectively, the flow vectors of the L and R subevents, and M_L and M_R are the corresponding multiplicities. Finally we get

$$c_n\{2\}_{\Delta\eta} = \langle\langle 2\rangle\rangle_{\Delta\eta} \quad \text{and } v_n\{2\}_{\Delta\eta} = \sqrt{c_n\{2\}_{\Delta\eta}}. \tag{14}$$

Instead of dividing an event into two subevents by inserting a pseudorapidity gap $\Delta\eta$, one can suppress the nonflow effects by exploiting the higher order multiparticle cumulants, expressed in the fourth order as

$$\begin{aligned}\langle 4\rangle = {} & [|Q_n|^4 + |Q_{2n}|^2 - 2\,\mathrm{Re}(Q_{2n}Q_n^*Q_n^*) \\ & - 2\{2(M-2)|Q_n|^2 \\ & - M(M-3)\}]/[M(M-1)(M-2)(M-3)],\end{aligned} \tag{15}$$

$$c_n\{4\} = \langle\langle 4\rangle\rangle - 2\langle\langle 2\rangle\rangle^2, \quad \text{and } v_n\{4\} = \sqrt[4]{-c_n\{4\}}. \tag{16}$$

The two- and four-particle cumulants have different contributions from flow fluctuations. In two-particle cumulants the contribution is positive and in four-particle cumulants it is negative. If the nonflow effects are negligible in two-particle cumulants, then $\sigma_{v_n} \ll \langle v_n\rangle$ and v_n in terms of fluctuation is given by [24]

$$v_n\{2\}^2 = \langle v_n\rangle^2 + \sigma_{v_n}^2 \quad \text{and } v_n\{4\}^2 = \langle v_n\rangle^2 - \sigma_{v_n}^2 \tag{17}$$

where $\langle v_n\rangle$ and σ_{v_n} are, respectively, the mean and standard deviation of the v_n distribution. From Eq. (17) the flow fluctuation and $\langle v_n\rangle$ can be estimated as

$$\sigma_{v_n} = \sqrt{\frac{v_n\{2\}^2 - v_n\{4\}^2}{2}} \tag{18}$$

and

$$\langle v_n\rangle\{\text{est}\} = \sqrt{\frac{v_n\{2\}^2 + v_n\{4\}^2}{2}}. \tag{19}$$

In a similar manner the cumulants of nth order eccentricity parameter ε_2 may also be defined [25] as

$$c_{\varepsilon_n}\{2\} = \langle\varepsilon_n^2\{PP\}\rangle, \tag{20}$$

$$c_{\varepsilon_n}\{4\} = \langle\varepsilon_n^4\{PP\}\rangle - 2\langle\varepsilon_n^2\{PP\}\rangle^2. \tag{21}$$

Here $\varepsilon_2\{PP\}$ represents the participant plane eccentricity calculated from Eq. (5). Corresponding cumulant based eccentricities are given by

$$\varepsilon_2\{2\} = \sqrt{c_{\varepsilon_2}\{2\}} \quad \text{and } \varepsilon_2\{4\} = \sqrt[4]{-c_{\varepsilon_2}\{4\}}. \tag{22}$$

We can estimate the eccentricity fluctuation σ_{ε_2} and the average eccentricity $\langle\varepsilon_2\rangle\{\text{est}\}$, by replacing $v_n\{2\}$ and $v_n\{4\}$, respectively, with $\varepsilon_2\{2\}$ and $\varepsilon_2\{4\}$ in Eqs. (18) and (19).

III. THE AMPT MODEL

The AMPT is a hybrid transport model that takes care of both hadronic and partonic degrees of freedom [11]. AMPT can be used over a very wide energy range, from low RHIC to LHC. In AMPT initial conditions, the spatial coordinates and momentum distributions of minijet partons and soft string excitations are obtained from HIJING [26]. The scattering of partons is modeled by the Zhang parton cascade (ZPC) scheme [27], with scattering cross sections taken directly from perturbative QCD where the gluon effective mass is set as a parameter. Depending upon the initial conditions, AMPT can be operated in two modes that implement two different hadronization schemes. In the AMPT default (AMPT-DEF) mode, minijet partons enter into the ZPC and once the partonic interactions cease to exist they recombine with their parent strings to form excited strings. Hadronization in the AMPT-DEF mode is described by the Lund string fragmentation scheme [28,29]. On the other hand, in the AMPT string melting (AMPT-SM) mode excited strings decompose into soft partons, and recombine with each other according to a quark coalescence scheme. Since inelastic scatterings are not included in the current version of the ZPC model, only quarks and antiquarks from melted strings are present. The final state hadronic scatterings are characterized by a relativistic transport model [30]. Transport models provide a microscopic description of the

early and late nonequilibrium stages of the fireball system. It has been observed that they significantly underpredict the v_2 values at the top RHIC energies. Inclusion of partonic degrees of freedom provides a more satisfactory result [31]. In a recent work an effort has been made to constrain the values of Lund string fragmentation parameters a and b and the parton scattering cross section (σ) with reference to the nucleus-nucleus collision experiments of the STAR collaboration at $\sqrt{s_{\rm NN}} = 7.7$, 27.0, and 200 GeV [32]. However, it has been observed that none of the parameter sets used in [32] can satisfactorily reproduce the p_T spectrum, the particle density at midrapidity, the particle yield and its ratio, as well as the flow parameters at all energies and for every species of particles.

IV. RESULTS AND DISCUSSION

In this section we present our simulation results on v_2 and its fluctuation σ_{v_2} obtained by using the AMPT-SM (v-2.26t9b) model. We have run the AMPT-SM code in the center of mass frame of the colliding nuclei, and set the parameters as $a = 0.55$, $b = 0.15$ GeV^{-2}, and $\sigma = 3$ mb [32]. With the current parameter setting the AMPT-SM model could predict the low-p_T results on charged pion and kaon yields, their p_T spectrum, and elliptic flow in central and midcentral ^{197}Au + ^{197}Au collisions at the top ($\sqrt{s_{\rm NN}} = 200$ GeV) RHIC energy [33]. Each minimum bias simulated sample consists of 10^7 events of ^{197}Au + ^{197}Au collision. The v_2 values obtained by using the participant plane method, the event plane method, and the two-particle and four-particle cumulant methods are denoted, respectively, by $v_2\{PP\}$, $v_2\{EP\}$, $v_2\{2\}$, and $v_2\{4\}$. We determine v_2 for charged hadrons with $p_T > 0.2$ GeV/c and falling within the central ($|\eta| < 1.0$) region. Collision centralities are determined by using the reference multiplicity ($N_{\rm ref}$) that takes care of the autocorrelation effect [34]. In our case $N_{\rm ref}$ denotes the multiplicity of charged hadrons that belong to the $|\eta| > 1.0$ region. In Fig. 1 we plot the centrality dependence of the simulated v_2 values obtained from the four methods mentioned above, along with the $v_2\{EP\}$, $v_2\{2\}$, and $v_2\{4\}$ values of the STAR experiment that are available in the literature [10]. In general, the shape of each AMPT-SM simulated plot of v_2 as a function of centrality matches with that of the respective experiment. At each $\sqrt{s_{\rm NN}}$ the minimum of v_2 values pertains to the most central collisions where the spatial anisotropy of the overlapping part of the colliding nuclei is minimum. Therefore, the effect of initial geometric anisotropy on the final state v_2 values is also minimum. The bell shape of the centrality dependence can be seen in the AMPT simulated plots of $v_2\{PP\}$ and $v_2\{4\}$. On the other hand, the centrality dependencies of $v_2\{EP\}$ and $v_2\{2\}$, that are almost always very closely valued to each other, exhibit a kind of saturation in the peripheral region, a feature that becomes more prominent with increasing $\sqrt{s_{\rm NN}}$. We note that in spite of good resemblances between the shapes of their distributions, often statistically significant differences are found in the integrated v_2 values obtained from the experiment and simulation. The fractional difference $|v_2(\text{STAR}) - v_2(\text{AMPT})|/v_2(\text{STAR})$ between the two varies over a wide range over the entire spectrum of centrality and $\sqrt{s_{\rm NN}}$, from as little as a few percent to as large as 45%. In most of the midcentral event classes, where the v_2 values are high, these differences are not too large ($\lesssim 10\%$) though. With increasing $\sqrt{s_{\rm NN}}$ the values of $v_2\{PP\}$ and $v_2\{4\}$ marginally become smaller than those of $v_2\{EP\}$ and $v_2\{2\}$. We notice at all energies the experimental values of $v_2\{EP\}$ and $v_2\{2\}$, and beyond $\sqrt{s_{\rm NN}} = 11.5$ GeV their simulated values almost overlap upon each other. This feature, as we shall also see in the subsequent discussion, is quite expected. We may note that a large number of neutral mesons are used to determine the event plane, which makes the effect of two-particle correlation vanishingly small in $v_2\{EP\}$ [12]. We also observe that by partitioning each event into two subevents separated by a gap of $\Delta\eta = 1.0$, it is possible to satisfactorily eliminate the SRC. Let us now examine to what extent the nonflow effect influences our $v_2\{2\}$ results in the AMPT-SM framework. To eliminate the nonflow effect, once again we divide each event into two subevents separated by an η gap of 1.0 and obtain the $v_2\{2\}$ values following the method prescribed by Eqs. (13) and (14). In Fig. 2 we plot $v_2\{2\}$ against percent centrality and compare the results on $v_2\{2\}$ with and without inserting an η gap. Except for a few extreme peripheral classes of events, two-particle correlation, the most dominant nonflow effect, does not significantly contribute to $v_2\{2\}$. With increasing energy one expects an enhancement in the minijet production which leads to an increase in $\delta v_2\{2\} = |v_2\{2\} - v_2\{2, \Delta\eta = 1.0\}|$, the difference in the $v_2\{2\}$ values obtained with and without inserting an η gap. In central collisions, due perhaps to multiple rescattering, the short-range effects are washed out and the $v_2\{2\}$ values obtained in two different ways practically overlap each other. Even in the peripheral collisions, where the rescattering effect is small, nonflow effects are not significantly high. In no case $\delta v_2\{2\}/v_2\{2\}$, the fractional difference, exceeds 20%. Similar observations are reported in small (p+Au, d+Au) as well as in large (Au+Au) systems at the RHIC energies [35,36], where the AMPT-SM model has been found to underestimate

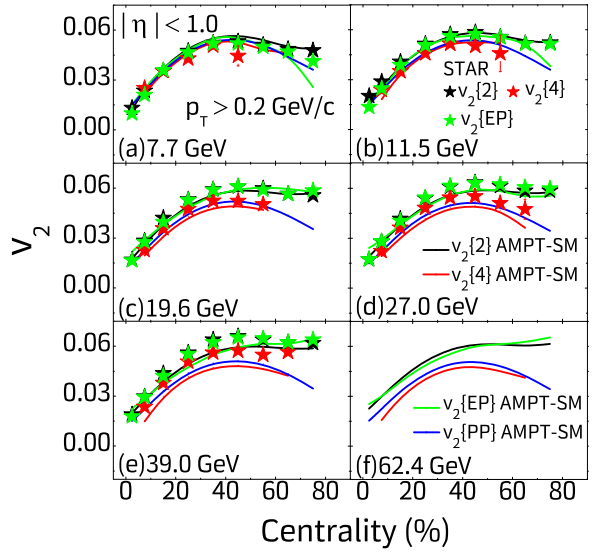

FIG. 1. Centrality dependence of v_2 for charged hadrons produced in ^{197}Au + ^{197}Au collisions at $\sqrt{s_{\rm NN}} = 7.7$, 11.5, 19.6, 27.0, 39.0, and 62.4 GeV. STAR experimental results are taken from [10].

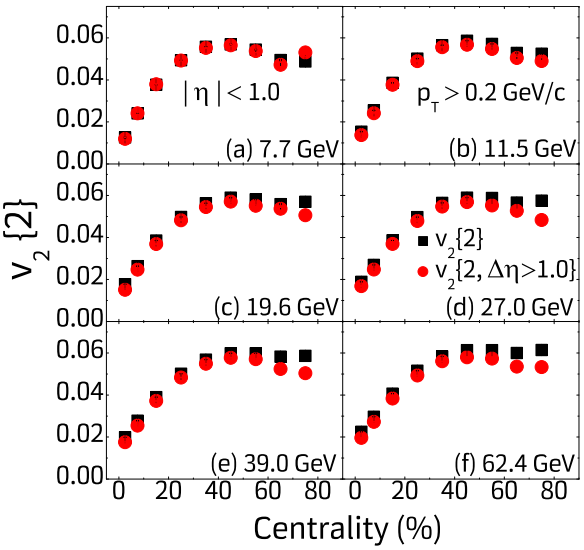

FIG. 2. Centrality dependence of $v_2\{2\}$ for the charged hadrons produced in ^{197}Au + ^{197}Au collisions with and without dividing an event into two subevents at $\sqrt{s_{\rm NN}} = 7.7$, 11.5, 19.6, 27.0, 39.0, and 62.4 GeV.

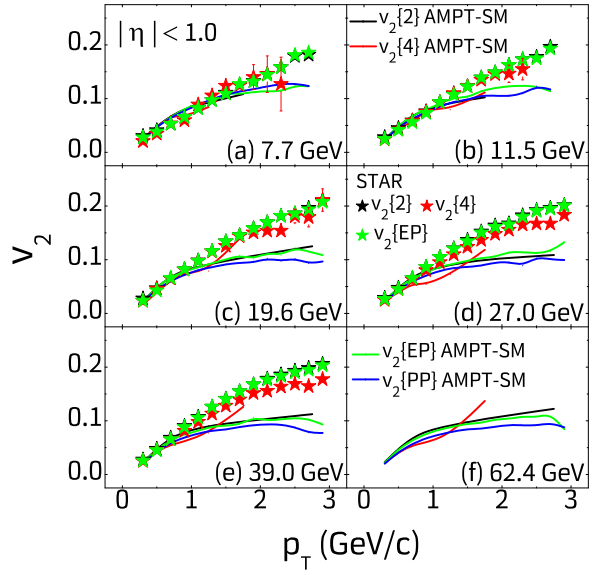

FIG. 3. p_T dependence of v_2 for the charged hadrons produced within the 20–30% centrality class in ^{197}Au + ^{197}Au collisions at $\sqrt{s_{\rm NN}} = 7.7$, 11.5, 19.6, 27.0, 39.0, and 62.4 GeV. STAR experimental results are taken from [10].

the experimentally observed nonflow effects. In a collision between two heavy nuclei, each binary NN collision should conserve the electric charge, baryon number, and strangeness, henceforth to be referred to only as charges. This means that oppositely charged particles are produced in pairs with small relative angles ($|\Delta\eta| < 1$) that would result in some extra correlations in the momenta of the produced particles [37]. It has been shown that the charge balancing indeed induces an additional component in the correlation function within a limited range ($|\Delta\eta| < 1$) [38], and therefore contributes to the nonflow source of $v_n\{2\}$ measured by the experiment [39]. The two-particle cumulants and correlators are sensitive to the charge conservation [40]. AMPT generated v_2 values obtained after taking the two-particle correlation into account [40] lie marginally below the $v_2\{2\}$ values reported by the ALICE experiment [41], but are in qualitative agreement with those expected when flow fluctuations and nonflow effects are suppressed. Though minijet and resonance production are present in the AMPT as two possible sources of SRC, the model does not efficiently handle the local conservation of charges as mentioned above, and therefore underpredicts the particle correlation.

In Fig. 3 we plot the p_T dependence of v_2 values obtained by using different methods. We observe the following.

(i) The experimental v_2 values almost linearly rise with p_T at all $\sqrt{s_{\rm NN}}$.

(ii) At 27.0 and 39.0 GeV, however, the $v_2(p_T)$ values tend to saturate at high p_T.

(iii) Values of $v_2\{EP\}$ and $v_2\{2\}$ almost overlap each other.

(iv) AMPT-SM simulation can reproduce the experiment only for the softest hadrons ($p_T < 1.0$ GeV/c).

(v) At high p_T the experimental $v_2\{4\}$ values are slightly smaller than those obtained by using other methods.

(vi) Beyond $p_T = 1.0$ GeV/c every AMPT-SM simulated $v_2(p_T)$ distribution underpredicts the respective experiment and saturates at all $\sqrt{s_{\rm NN}}$ and for all methods of v_2 determination.

The tendency of the experimental v_2 values to saturate at 27.0 and 39.0 GeV may be attributed to a mixed (partonic+hadronic) intermediate phase, a feature that is also observed in ^{197}Au + ^{197}Au experiments at the top RHIC energies [42]. It has been noted that at high p_T the AMPT-SM may not be quite reliable to generate a sufficient amount of collective flow as it lacks inelastic collisions among the partons [43]. The radiative energy loss suffered by the high-p_T partons is missing in the model. Partonic inelastic scattering is necessary to bring the evolution of the fireball system closer to that of an ideal hydrodynamics, which requires a pressure anisotropy to develop and to be maintained [44]. Hydrodynamical calculations [45,46], that are otherwise quite successful to predict the p_T dependence of v_2 of identified charged hadrons [47], assume the fireball in local thermal equilibrium. In traditional methods of hydrodynamic evolution, one first averages over many fluctuating initial profiles to obtain a smooth average asymmetric profile, which then evolves hydrodynamically to result in a final state momentum anisotropy. However, large v_2 values observed in the RHIC experiments suggest a very short ($\approx$1 fm/c) equilibration time, which in the framework of perturbative QCD is difficult to reconcile [9], where the early rapid expansion of the fireball is considered to be closer to free streaming than hydrodynamic evolution.

In Fig. 4 we schematically represent the v_2 distributions against η for the charged hadrons produced within the 10–40% centrality class. STAR experimental values of $v_2\{EP\}$ are plotted along with the AMPT-SM simulated values of $v_2\{EP\}$. Values of $v_2\{2\}$ and $v_2\{PP\}$ are also incorporated. AMPT-SM consistently underpredicts the experiment. Fractional difference between the two increases from about 14% at 7.7 GeV to about 24% at 62.4 GeV. Unlike in the

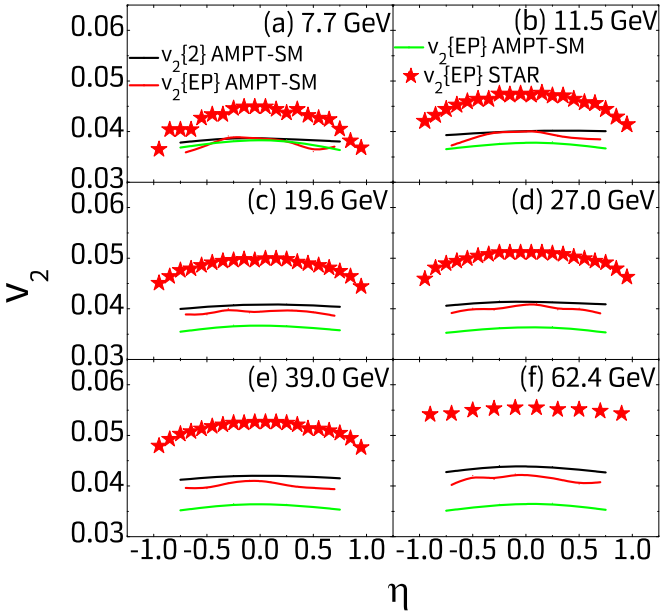

FIG. 4. Pseudorapidity dependence of v_2 for charged hadrons produced within the 10–40% centrality class in ^{197}Au + ^{197}Au collisions at $\sqrt{s_{\rm NN}} = 7.7$, 11.5, 19.6, 27.0, 39.0, and 62.4 GeV. STAR experimental results are taken from [10].

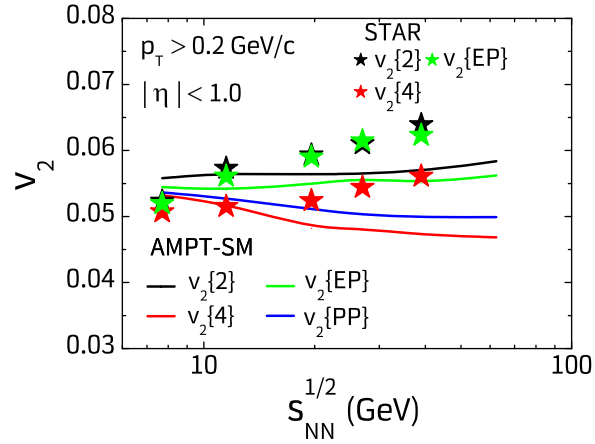

FIG. 5. Energy dependence of v_2 for the charged hadrons produced within the 30–40% centrality class in ^{197}Au + ^{197}Au collisions at $\sqrt{s_{\rm NN}} = 7.7$, 11.5, 19.6, 27.0, 39.0, and 62.4 GeV. STAR experimental results are taken from [10].

experiment, the simulated $v_2(\eta)$ values remain almost always uniformly distributed. At lower collision energies $v_2\{EP\}$ and $v_2\{2\}$ values are very close to each other. As the energy increases small differences start appearing between the two. $v_2\{2\}$ marginally exceeds $v_2\{EP\}$, which indicates a growing influence of the nonflow effects. Observed differences in the $v_2(\eta)$ distributions may be attributed to insufficient inelastic collisions among the partons in AMPT-SM, which as pointed out before leads to a smaller elliptic flow. A study showed that, compared to the equation of state (EoS) of the lattice QCD, quark coalescence starts too late in the AMPT-SM, when the energy densities are much less than 1 GeV/fm^3 [44]. The effective EoS of the AMPT-SM would have been more realistic if the parton recombination had been implemented according to the local energy densities, which would have lead to a more efficient parton recombination (hadronization) [48]. We find that the density of charged hadrons (pions, kaons, and protons) in the central ($\eta = 0$) region increases almost linearly with $\sqrt{s_{\rm NN}}$ both in the simulation and in the experiment. However, at lower $\sqrt{s_{\rm NN}}$ the AMPT-SM overpredicts $dN_{\rm ch}/d\eta$, whereas at higher energies it underpredicts the particle densities obtained from the experiment. A higher particle density means a higher probability of interaction which in turn generates a larger collective flow. The differences between the AMPT generated and experimental particle densities only add to the observed differences between the simulated and experimental $v_2\{EP\}$ values. In Fig. 5 we plot the v_2 values against $\sqrt{s_{\rm NN}}$ for the 30–40% centrality. We observe that the experimental v_2 values marginally grow with energy, the rise being almost linear. With increasing $\sqrt{s_{\rm NN}}$ the simulated values on the other hand either remain uniformly distributed, as in $v_2\{EP\}$ or $v_2\{2\}$, or decrease marginally as in $v_2\{PP\}$ or $v_2\{4\}$. Once again the experimental $v_2\{EP\}$ values nicely match with the $v_2\{2\}$ values, whereas $v_2\{4\}$ remains consistently lower than the two. Contribution of high-p_T hadrons should grow with increasing $\sqrt{s_{\rm NN}}$. We have already seen that at high p_T, AMPT-SM grossly underestimates the differential distribution of $v_2(p_T)$ obtained from the experiment. With increasing $\sqrt{s_{\rm NN}}$ not only the difference between the simulation and experiment widens, but the departure of one from the other starts at lower p_T. These two aspects of the differential distribution together affect similarly the integrated values. Similar observation on the $\sqrt{s_{\rm NN}}$ dependence of v_2 in the framework of AMPT-SM has been made in [31]. We next obtain the σ_{v_2} values using Eq. (18) and in Fig. 6 plot them as a function of collision centrality. The AMPT-SM results, with and without taking the

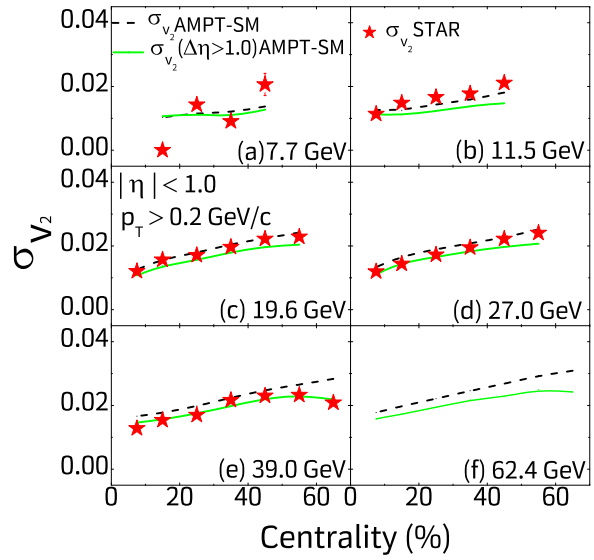

FIG. 6. Centrality dependence of the elliptic flow fluctuation (σ_{v_2}) for the charged hadrons produced in ^{197}Au + ^{197}Au collisions with and without taking the nonflow effects into account at $\sqrt{s_{\rm NN}} =$ 7.7, 11.5, 19.6, 27.0, 39.0, and 62.4 GeV. STAR experimental results with nonflow effects are estimated from [10].

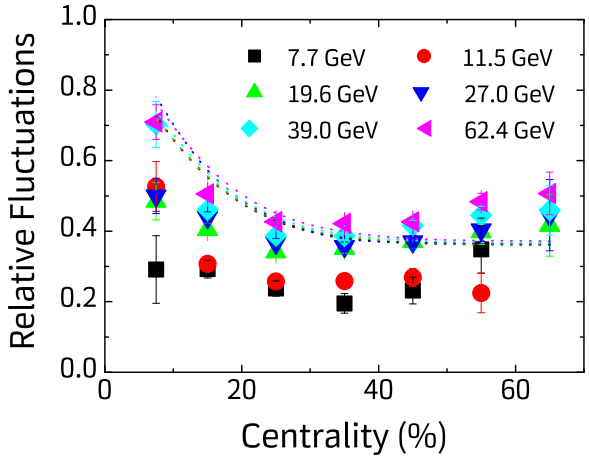

FIG. 7. AMPT generated relative fluctuations of v_2 and ε_2 in ^{197}Au + ^{197}Au collisions are plotted against centrality. The points represent $\sigma_{v_2}/\langle v_2\rangle\{\text{est}\}$ and the dotted lines represent $\sigma_{\varepsilon_2}/\langle\varepsilon_2\rangle\{\text{est}\}$ following the same color code of points.

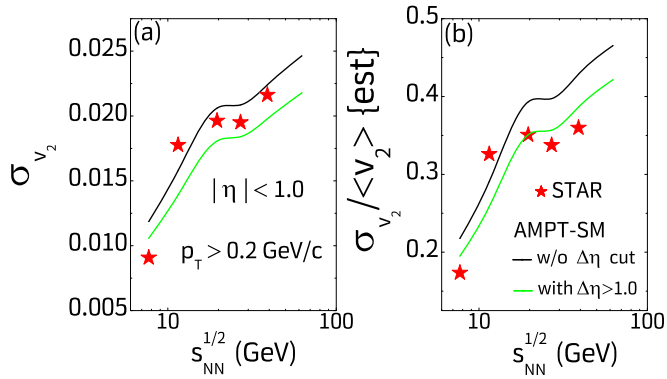

FIG. 8. Energy dependence of the v_2 fluctuation and corresponding relative fluctuation for the charged hadrons falling within the 30–40% centrality class in ^{197}Au + ^{197}Au collisions. STAR experimental results with nonflow effects are estimated from [10].

SRC into account, are compared with the STAR experimental results on σ_{v_2} estimated from [10], where nonflow effects originating from the SRC are present. We find that in all cases fluctuations in v_2 increase from central to peripheral collisions, and in AMPT-SM the SRC raises the amount of σ_{v_2} only by a very small amount. Barring $\sqrt{s_{\text{NN}}} = 7.7$ GeV at all other energies the agreement between the experiment and corresponding simulation is quite satisfactory. In Fig. 7 we plot the relative fluctuation $\sigma_{v_2}/\langle v_2\rangle\{\text{est}\}$ against centrality. $\langle v_2\rangle\{\text{est}\}$ is obtained from Eq. (19) and the SRC is eliminated by inserting a gap of $\Delta\eta = 1.0$ in between the subevents. We see an energy ordering; in general $\sigma_{v_2}/\langle v_2\rangle\{\text{est}\}$ increases with increasing $\sqrt{s_{\text{NN}}}$. At all energies excepting 7.7 GeV, $\sigma_{v_2}/\langle v_2\rangle\{\text{est}\}$ is largest for the most central class of events. From the most central class $\sigma_{v_2}/\langle v_2\rangle\{\text{est}\}$ falls off either to attain a saturation or to rise marginally once again towards semiperipheral and peripheral classes of events. At $\sqrt{s_{\text{NN}}} =$ 7.7 GeV, within statistical uncertainties, $\sigma_{v_2}/\langle v_2\rangle\{\text{est}\}$ is more or less uniformly distributed. In the same diagram we also incorporate the centrality dependence of the relative fluctuation of the eccentricity parameter ($\sigma_{\varepsilon_2}/\langle\varepsilon_2\rangle\{\text{est}\}$) of the overlapping part of the colliding nuclei. Their values are obtained by using the MCG model [17]. Since the eccentricity is an initial state parameter, its fluctuation should not depend upon how the collision dynamics evolves with space-time. We also note that, within the energy range considered in our analysis, the experimentally measured NN inelastic scattering cross sections used in the MCG simulation fluctuate nominally about a mean value $\sigma_{\text{NN}}^{\text{inel}} = 31.5$ mb [49]. As a result, the average number of participating nuclei $N_{\text{participant}}$ also depends weakly upon collision energy within $7.7 \leqslant \sqrt{s_{\text{NN}}} \leqslant$ 62.4 GeV. Therefore, the eccentricity values and their e-by-e fluctuations are found to vary marginally in the present analysis. A similar type of near energy independence of the Glauber model generated eccentricity values has been reported elsewhere [50]. As expected, we do not find any significant energy dependence of $\sigma_{\varepsilon_2}/\langle\varepsilon_2\rangle\{\text{est}\}$ either (Fig. 7). However, starting from an initial value of about 75% for the 5–10% most central events $\sigma_{\varepsilon_2}/\langle\varepsilon_2\rangle\{\text{est}\}$ values fall off gradually to saturate down to about 40% towards the peripheral events.

We now examine the energy dependencies of v_2 fluctuation and its relative fluctuation in Fig. 8. The STAR experimental values are plotted along with the AMPT-SM simulation results with and without taking the SRC into account. The plots are made for the 30–40% most central events, where elliptic flow is near its maximum. We see that both σ_{v_2} and $\sigma_{v_2}/\langle v_2\rangle\{\text{est}\}$ depend nonmonotonically on $\sqrt{s_{\text{NN}}}$ in the simulation(s) as well as in the experiment. Both of them initially rise with energy, remain almost uniform over a range, and then again show a rising trend. We see qualitative agreement between the experiment and simulation(s) in their nature of variation. Particularly in Fig. 8(b), $\sigma_{v_2}/\langle v_2\rangle\{\text{est}\}$ shows an almost energy independence in the $11.5 \leqslant \sqrt{s_{\text{NN}}} \leqslant 27.0$ GeV range.

Hydrodynamic calculations suggest that v_2 should linearly scale with ε_2, and σ_{v_2} should therefore scale with σ_{ε_2} [7,51]. In order to scrutinize the influence of σ_{ε_2} on σ_{v_2}, we take $\sqrt{s_{\text{NN}}} = 27.0$ GeV as a representative case. In Fig. 9 we plot (a) the centrality dependence of ε_2, (b) the ratio v_2/ε_2 against centrality, and (c) σ_{v_2} against σ_{ε_2} for the AMPT-SM with and without taking the SRC into account. In Fig. 9(c) we incorporate the STAR experimental results. We observe an almost linear dependence of ε_2 on the percentile centrality, which simply implies that the initial spatial anisotropy increases from central to peripheral collisions. We notice that in the semiperipheral and peripheral collisions $\varepsilon_2\{2\} > \varepsilon_2\{PP\} > \varepsilon_2\{4\}$. We may recall that in our simulation the centrality dependence of v_2 was not linear. We see that in the AMPT-SM model, except for a limited centrality range ($< 20\%$), the v_2/ε_2 ratio decreases linearly with increasing centrality. In this regard AMPT is quite similar to the hydrodynamics prediction [52], where the v_2/ε_2 ratio is found to decrease with increasing centrality. In Fig. 9(c) we see that the centrality dependencies of σ_{v_2} in the AMPT-SM, with and without SRC, and σ_{v_2} of the STAR experiment with SRC, are reasonably well reproduced by the centrality dependence of σ_{ε_2}. It appears that fluctuations in ε_2 contribute significantly to the experimentally observed and simulated fluctuations in v_2. However, looking

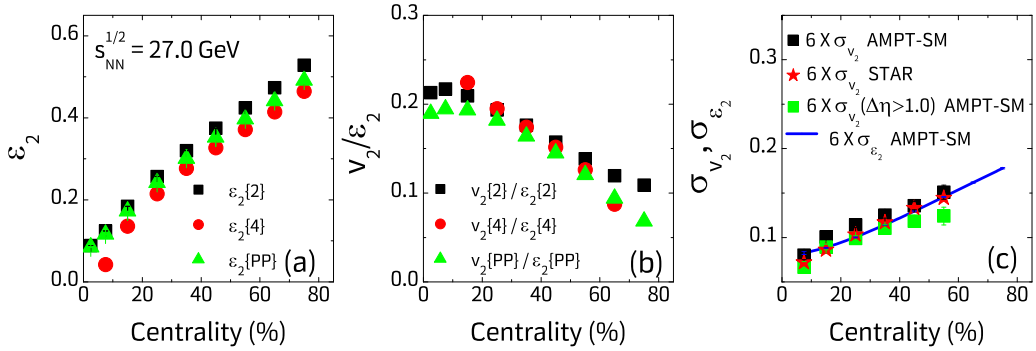

FIG. 9. (a) Centrality dependence of the eccentricity (ε_2), (b) that of the elliptic flow fluctuation (σ_{ε_2}), and (c) ε_2 scaling of v_2 in ^{197}Au + ^{197}Au collisions at $\sqrt{s_{NN}} = 27.0$ GeV in AMPT-SM. STAR experimental results with nonflow effects [10] are incorporated in (c).

at the energy ordering of σ_{v_2}/v_2 in Fig. 7, we may conclude that not only the initial geometrical fluctuations, but fluctuations in the dynamical evolution of the fireball system, as well as the v_2 values themselves also play important roles to develop the v_2 fluctuations at the final states of high-energy heavy-ion collisions. As far as the linear scaling between v_2 and ε_2 is concerned, except for the most central collisions our AMPT-SM results are similar to the predictions of hydrodynamics [52].

V. CONCLUSIONS

In this paper we use the predictions of the AMPT-SM model as a reference baseline, and study the elliptic flow and e-by-e fluctuation of the elliptic flow of charged hadrons produced in ^{197}Au + ^{197}Au collisions at $\sqrt{s_{NN}} = 7.7$–62.4 GeV. We adopt different methods to determine the v_2 parameter. In particular, we intend to take care of the nonflow fluctuations present in v_2 originating from SRC. We compare the experimental results obtained from the STAR-BES phase I program with our simulated results. We observe that the AMPT-SM, predominantly partonic in nature, can qualitatively reproduce the nature of centrality dependence of v_2 observed in the experiment. However, quantitatively the model, with its present parameter setting, underestimates the experimental v_2 values. Contribution of nonflow effects is found to be marginal in this regard. The simulation underpredicts the differential distribution of v_2 against p_T except at very low values ($p_T < 1.0$ GeV/c), and it also grossly underpredicts the distribution of v_2 against η. Experimental v_2 values marginally increase with $\sqrt{s_{NN}}$. The simulated values, on the other hand, either remain uniformly distributed or marginally decrease with increasing energy. Beside fine tuning the parameter setting, we believe that noninclusion of inelastic parton rescattering, a rather delayed hadronization through the quark coalescence mechanism, and nonconservation of charges in the AMPT-SM are responsible for the observed discrepancies between the simulation and the experiment. Fluctuations in v_2 slowly and almost linearly increase from central to peripheral collisions. Except at $\sqrt{s_{NN}} = 7.7$ GeV, each experiment in this regard matches reasonably well with the respective simulation. Once the two-particle correlation is taken care of, the contribution of nonflow effect to σ_{v_2} appears to be marginal. The increasing trend of σ_{v_2} from central to peripheral events is perhaps a multiplicity effect. The relative fluctuations in v_2 show an energy ordering. This may be attributed to multiple rescattering among the final state hadrons, which should increase with the collision energy. It is quite interesting to notice that both the e-by-e fluctuation of v_2 and its relative fluctuation show a nonmonotonic $\sqrt{s_{NN}}$ dependence. It remains an open question whether some nontrivial physics issue is involved with the apparent suppression of σ_{v_2}/v_2 within a limited energy range, or it is merely an artifact of the method(s) employed to determine the v_2 parameters. At $\sqrt{s_{NN}} = 27.0$ GeV we observe an eccentricity scaling of v_2 only for the central (<20% centrality) collisions, where multiple rescattering is expected to be high, an essential condition to achieve any kind of equilibration. Beyond 20% centrality the prediction of AMPT-SM behaves quite similarly to the hydrodynamic expectation. However, σ_{v_2}, with and without SRC, appears to scale with σ_{ε_2} reasonably well, both in the simulation and in the experiment. We learn that the e-by-e fluctuations in v_2 are sensitive to both the initial state fluctuations and those occurring during the evolution of the collision process. Moreover, the relative fluctuations in v_2 are influenced by the initial fluctuations, the fluctuations during evolution, and the flow magnitude.

ACKNOWLEDGMENTS

J.T. acknowledges the financial assistance received in the form of a senior research fellowship of North Bengal University (Grant No. 1054-R/2019) funded by the Government of West Bengal.

[1] K. Adcox *et al.* (PHENIX Collaboration), Nucl. Phys. A **757**, 184 (2005).

[2] J. Adams *et al.* (STAR Collaboration), Nucl. Phys. A **757**, 102 (2005).

[3] B. Alver *et al.* (PHOBOS Collaboration), Phys. Rev. Lett. **98**, 242302 (2007).
[4] K. Aamodt *et al.* (ALICE Collaboration), Phys. Rev. Lett. **105**, 252302 (2010).
[5] S. Voloshin and Y. Zhang, Z. Phys. C **70**, 665 (1996).
[6] H. Sorge, Phys. Rev. Lett. **78**, 2309 (1997).
[7] G. Agakishiev *et al.* (STAR Collaboration), Phys. Rev. C **86**, 014904 (2012).
[8] C. Loizides (for the PHOBOS Collaboration), J. Phys. G **34**, S907-S910 (2007).
[9] S. Mrowczynski and E. Shuryak, Acta Phys. Polon. B **34**, 4241 (2003).
[10] L. Adamczyk *et al.* (STAR Collaboration), Phys. Rev. C **86**, 054908 (2012).
[11] Z.-W. Lin, C. M. Ko, B.-A. Li, B. Zhang, and S. Pal, Phys. Rev. C **72**, 064901 (2005).
[12] A. M. Poskanzer and S. A. Voloshin, Phys. Rev. C **58**, 1671 (1998).
[13] S. Wang, Y. Z. Jiang, Y. M. Liu, D. Keane, D. Beavis, S. Y. Chu, S. Y. Fung, M. Vient, C. Hartnack, and H. Stöcker, Phys. Rev. C **44**, 1091 (1991).
[14] N. Borghini, P. M. Dinh, and J.-Y. Ollitrault, Phys. Rev. C **63**, 054906 (2001).
[15] N. Borghini, P. M. Dinh, and J.-Y. Ollitrault, Phys. Rev. C **64**, 054901 (2001).
[16] R. S. Bhalerao, N. Borghini, and J.-Y. Ollitrault, Nucl. Phys. A **727**, 373 (2003).
[17] M. L. Miller, K. Reygers, S. J. Sanders, and P. Steinberg, Annu. Rev. Nucl. Part. Sci. **57**, 205 (2007).
[18] B. Alver and G. Roland, Phys. Rev. C **81**, 054905 (2010).
[19] L. X. Han, G. L. Ma, Y. G. Ma, X. Z. Cai, J. H. Chen, S. Zhang, and C. Zhong, Phys. Rev. C **83**, 047901 (2011).
[20] P. Danielewicz and G. Odyniec, Phys. Lett. B **157**, 146 (1985).
[21] A. Bilandzic, R. Snellings, and S. Voloshin, Phys. Rev. C **83**, 044913 (2011).
[22] Y. Zhou (ALICE Collaboration), Nucl. Phys. A **931**, 949 (2014).
[23] G. J. Alner *et al.*, Phys. Rep. **154**, 247 (1987).
[24] S. Voloshin, A. Poskanzer, A. Tang, and G. Wang, Phys. Lett. B **659**, 537 (2008).
[25] L. Ma, G. L. Ma, and Y. G. Ma, Phys. Rev. C **94**, 044915 (2016).
[26] X. N. Wang and M. Gyulassy, Phys. Rev. D **44**, 3501 (1991).
[27] B. Zhang, Comput. Phys. Commun. **109**, 193 (1998).
[28] B. Andersson, G. Gustafson, and B. Soderberg, Z. Phys. C **20**, 317 (1983).
[29] B. Andersson, G. Gustafson, G. Ingelman, and T. Sjostrand, Phys. Rep. **97**, 31 (1983).
[30] B. A. Li and C. M. Ko, Phys. Rev. C **52**, 2037 (1995).
[31] M. Nasim, L. Kumar, P. K. Netrakanti, and B. Mohanty, Phys. Rev. C **82**, 054908 (2010).
[32] A. Nandi, L. Kumar, and N. Sharma, Phys. Rev. C **102**, 024902 (2020).
[33] Z.-W. Lin, Phys. Rev. C **90**, 014904 (2014).
[34] S. De, T. Tarnowsky, T. K. Nayak, R. P. Scharenberg, and B. K. Srivastava, Phys. Rev. C **88**, 044903 (2013).
[35] C. Aidala *et al.* (PHENIX Collaboration), Phys. Rev. Lett. **120**, 062302 (2018).
[36] Y. Zhou, K. Xiao, Z. Feng, F. Liu, and R. Snellings, Phys. Rev. C **93**, 034909 (2016).
[37] P. Bożek, Phys. Lett. B **609**, 247 (2005).
[38] P. Bożek and W. Broniowski, Phys. Rev. Lett. **109**, 062301 (2012).
[39] K. Aamodt *et al.* (ALICE Collaboration), Phys. Rev. Lett. **107**, 032301 (2011).
[40] S. Basu, V. Gonzalez, J. Pan, A. Knospe, A. Marin, C. Markert, and C. Pruneau, Phys. Rev. C **104**, 064902 (2021).
[41] B. B. Abelev *et al.* (ALICE Collaboration), Phys. Rev. C **90**, 054901 (2014).
[42] S. S. Adler *et al.* (PHENIX Collaboration), Phys. Rev. Lett. **94**, 232302 (2005).
[43] Z.-W. Lin and L. Zheng, Nucl. Sci. Tech. **32**, 113 (2021).
[44] B. Zhang, L.-W. Chen, and C. M. Ko, J. Phys. G **35**, 065103 (2008).
[45] P. F. Kolb, J Sollfrank, and U. W. Heinz, Phys. Rev. C **62**, 054909 (2000).
[46] P. Huovinen, P. F. Kolb, U. Heinz, P. V. Ruuskanen, and S. A. Voloshin, Phys. Lett. B **503**, 58 (2001).
[47] C. Adler *et al.* (STAR Collaboration), Phys. Rev. Lett. **87**, 182301 (2001).
[48] Z.-W. Lin, Acta Phys. Pol. B Proc. Suppl. **7**, 191 (2014).
[49] P. A. Zyla *et al.* (Particle Data Group), Prog. Theor. Exp. Phys. **2020**, 083C01 (2020).
[50] X. Y. Wu, G. Y. Qin, L. G. Pang, and X. N. Wang, Phys. Rev. C **105**, 034909 (2022).
[51] H. Niemi, G. S. Denicol, H. Holopainen, and P. Huovinen, Phys. Rev. C **87**, 054901 (2013).
[52] H. Song, S. A. Bass, U. Heinz, T. Hirano, and C. Shen, Phys. Rev. Lett. **106**, 192301 (2011).